Membrane-on-a-Chip: Microstructured Silicon/Silicon-Dioxide Chips for High-Throughput Screening of Membrane Transport and Viral Membrane Fusion

Ilja Kusters,[†] Antoine M. van Oijen,[‡] and Arnold J. M. Driessen[†,*]

[†]Department of Microbiology, Groningen Biomolecular Sciences and Biotechnology Institute and the Zernike Institute for Advanced Materials, University of Groningen, Nijenborgh 7, Groningen, The Netherlands and [‡]Single Molecule Biophysics, Zernike Institute for Advanced Materials and Center for Synthetic Biology, University of Groningen, Nijenborgh 4, Groningen, The Netherlands

ABSTRACT Screening of transport processes across biological membranes is hindered by the challenge to establish fragile supported lipid bilayers and the difficulty to determine at which side of the membrane reactants reside. Here, we present a method for the generation of suspended lipid bilayers with physiological relevant lipid compositions on microstructured Si/SiO_2 chips that allow for high-throughput screening of both membrane transport and viral membrane fusion. Simultaneous observation of hundreds of single-membrane channels yields statistical information revealing population heterogeneities of the pore assembly and conductance of the bacterial toxin α-hemolysin (αHL). The influence of lipid composition and ionic strength on αHL pore formation was investigated at the single-channel level, resolving features of the pore-assembly pathway. Pore formation is inhibited by a specific antibody, demonstrating the applicability of the platform for drug screening of bacterial toxins and cell-penetrating agents. Furthermore, fusion of H3N2 influenza viruses with suspended lipid bilayers can be observed directly using a specialized chip architecture. The presented micropore arrays are compatible with fluorescence readout from below using an air objective, thus allowing high-throughput screening of membrane transport in multiwell formats in analogy to plate readers.

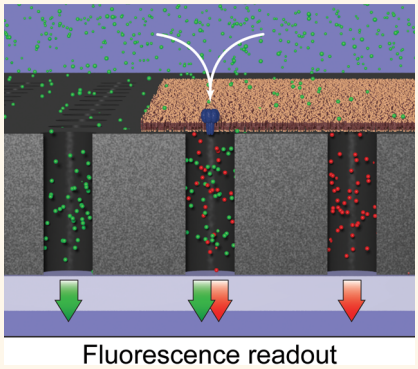

KEYWORDS: micropore array · suspended lipid bilayers · membrane transport · virus fusion · α-hemolysin

Detailed investigations of transport processes across biological membranes as well as drug screening approaches utilizing membrane protein targets are hindered by the intrinsic difficulty to handle immobilized lipid bilayers such that the embedded membrane proteins remain active. Although 60% of the human drug targets are membrane proteins, assays to probe their activity in their native environment are rare and technically demanding.[1] Ideally, stable lipid bilayers are generated in an analytical setup that allows automated readout of a multitude of individual membrane transport events combined with simple sample preparation. Such an approach would enable drug screening approaches against membrane-associated targets such as toxins, transporters, or membrane-penetrating viruses. Moreover, the effect of cell-penetrating and pore-forming antimicrobial peptides could be studied.

Traditionally, membrane transport is probed by the uptake and efflux of radioactively or fluorescently labeled substrates, whereupon transport is followed after filtration or by fluorescence spectroscopy. Due to ensemble averaging in such bulk assays, important details such as number of active transporters, individual conductances, and population heterogeneity are lost. In order to reveal such specifics of transport processes, synchronization of reactions or spatiotemporal separation of individual transport events needs to be achieved. Direct observation of biological membranes and embedded

* Address correspondence to a.j.m.driessen@rug.nl.

Received for review November 13, 2013 and accepted March 6, 2014.

Published online March 06, 2014
10.1021/nn405884a

transporters can be realized using surface-supported lipid bilayers.[2,3] The lateral mobility of lipids in a glass-supported bilayer is maintained due to a 1−2 nm water layer between the membrane and the hydrophilic surface.[2] When membrane proteins are embedded, the bilayer needs to be cushioned by polymers or hydrogels to avoid contact between the protein and the glass surface.[3] While this technique allows observation of individual membrane proteins or bound viruses, it does not permit recording the activity of single transporters and channels over a longer period of time, as the aqueous medium on the cis- and trans-side of the membrane is continuous and transported molecules diffuse freely. Moreover, it is challenging to optically resolve the space above and below the membrane to determine transport processes. The same problem applies to surface-adsorbed membrane vesicles that are too small to determine the transport into their lumen.

An attractive alternative would be the use of surface-supported planar lipid bilayers assembled into a setup in which the cis- and trans-side of the membrane can be monitored separately. Lipid bilayers separating compartments large enough to be resolved by light microscopy are therefore ideal for the quantitative detection of membrane transport processes. The groups of Tampé and Steinem pioneered the generation of suspended lipid bilayers spanning cavities of nanopore arrays. Herein, nanopore arrays were fabricated by electron-beam lithography, while stable lipid bilayers could be formed on top of the <100 nm pores.[4] Leakage of a fluorophore entrapped in bilayer-sealed cavities was used to detect membrane pore formation. Although very accurate and sophisticated nanopore arrays can be created by electron-beam lithography, the rather difficult manufacturing process leads to low piece counts and high production costs. A different approach was taken by the Steinem group that sealed porous anodic aluminum oxide with lipid bilayers upon rupture of giant unilamellar vesicles (GUVs).[5] Due to the transparent nature of the material, fluorescent dyes inside the pores and above the chip can be detected by confocal laser-scanning microscopy. However, since the 60 nm pores are densely packed, readout of individual pores is impossible due to the diffraction limit. Another strategy was used to prepare suspended lipid bilayers by GUV rupture using gold and mercaptoethanol functionalized silicon nitride pores with 1.2 μm diameter.[6] A major disadvantage of all above-mentioned nano- and micropore strategies is that the fluorescence readout must occur from the aqueous environment above the chip. Thus, cleaning of the objective lens is required after each measurement, complicating high-throughput analysis of multiple chips. Furthermore, a large aqueous volume is required to accommodate the objective, increasing the sample volume substantially.

Here we present a next generation of microstructured Si/SiO_2 chips that enable high-throughput analysis of membrane transport and membrane fusion events. Due to the design and optical properties of the chips, fluorescence readout is possible from below using air objectives and CCD cameras. This format allows measurements of multiple chips attached to the bottom of multiwell sample holders using automated microscopes similar to plate readers. Furthermore, the chips are entirely manufactured by reactive ion etching, a technique amenable for mass production. We demonstrate that suspended lipid bilayers on micropore arrays allow simultaneous recordings of hundreds of single-membrane channels embedded in a variety of synthetic and native membranes. In addition, the suspended lipid bilayers were employed to analyze membrane mixing upon membrane fusion of H3N2 influenza viruses.

RESULTS

Si/SiO_2 Micropore Arrays for Selective Fluorescent Readout. Micropore arrays are a new tool for the detection of translocation processes of fluorescent or fluorescently labeled substrates across biological membranes. The here-presented commercially available Si/SiO_2 chips contain an array of thousands of cylindrical measurement chambers (0.85 μm × 10 μm) in a silicon layer bound to an unstructured 160 μm thick glass support. The silicon-glass chip is attached to the ∼100 μm thick glass bottom of an eight-well sample holder with optically transparent and nonfluorescent glue (∼20 μm) and compatible with fluorescent readout from below using objectives with working distances of 300 μm or above (Figure 1A). The microcavities in the silicon layer, generated by reactive ion etching, are arranged in a regular matrix with a center-to-center distance of 4 μm (Figure 1B,C). Using a 20× air objective and a 1.45 megapixel CCD camera, around 8800 cavities can be observed simultaneously (supplementary video SV1). Suspended lipid bilayers spanning the cavities of the chip were generated by rupture of giant unilamellar vesicles. To this end, GUVs were obtained by swelling of a dried lipid film in a dextran-containing buffer[7,8] and transferred to the well with the hydrated chip. The dextran in the GUV lumen leads to a slow sedimentation, while bivalent cations such as Ca^{2+} and Mg^{2+} in the buffer mediate the attachment to the Si/SiO_2 chip surface that supports the bilayer (Figure 1B, supplementary Figure S1). A short centrifugation of the chip leads to rupture of the GUVs and formation of planar lipid bilayers spanning the cavities of the chip. In this manner, fluorophores added to the chip prior to GUV collapse are entrapped in the cavities by the bilayer and serve to identify sealed areas (Figure 1B−D, supplementary Figures S1 and S2A). As silicon is transparent in the red light spectrum, intact GUVs can be observed by phase

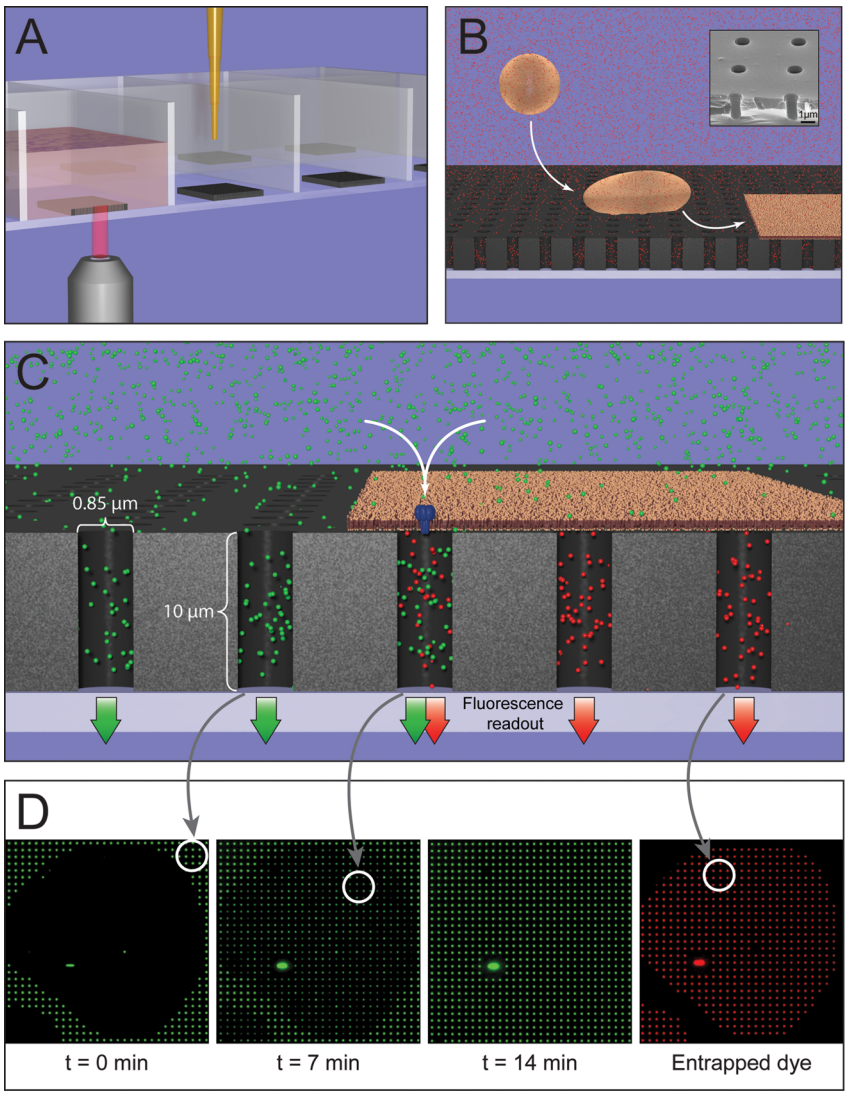

Figure 1. Principle of membrane transport measurements with microstructured silicon chips. (A) Experimental setup; microstructured Si/SiO_2 chips in a multiwell sample holder are compatible with automated microscopes and pipetting robotics. Illumination and fluorescence detection is accomplished from below. Due to the optical properties of the chip, only fluorophores inside the cavities (6.5 fL) are excited, allowing high substrate concentration above the chip. (B) Formation of a free-standing lipid bilayer. Giant unilamellar vesicles (GUVs) collapse on a microporous chip such that the lipid bilayer spans the cavities leading to entrapment of a fluorophore. Bilayer-sealed areas are identified by fluorophore entrapment after washing. Inset: SEM image of E800 chip. (C) A fluorescent substrate added after establishment of the lipid bilayer seal is imported by a membrane transporter. Imaging of entrapped sealing-control fluorophore (red), transport substrate (green), and lipid-embedded dye allows discriminating between transport, leakage, and membrane rupture. (D) Insertion of αHL pores leads to diffusion of the green transport dye into the bilayer-sealed cavities.

contrast microscopy as a control for bilayer formation (supplementary Figure S1).

Stability of Suspended Lipid Bilayers. The lipid bilayer generated by GUV rupture was visualized from the top by fluorescence imaging of the incorporated lipid dye Atto647-DOPE (1,2-dioleoyl-*sn*-glycero-3-phosphoethanolamine) (Figure S2A). Interestingly, the bilayer areas in contact with the silicon support displayed a quenched fluorescence of Atto647-DOPE consistent with previous observations of fluorescence quenching close to silicon surfaces,[9] while the dye in suspended membranes is normally fluorescent (Figure S2A). The stability of the bilayer was probed by measuring both efflux of an entrapped fluorophore and influx of a fluorophore added after formation of the bilayer seal. At all tested osmotic strength values (40−340 mOsm/L) at least 99.7% of the initially sealed cavities did not show any significant fluorescence changes after 16 h, confirming the stability of the bilayer seal (Figure S2B). By imaging the bilayer-sealed areas from below, the optical properties of the chip can be illustrated. Due to the nontransparent nature of silicon below 650 nm and the narrow geometry of the cavities, only very little excitation light from below reaches the buffer above the chip that contains high fluorophore concentrations (typically 1−10 μM).

Thus, bilayer-sealed cavities do not show any fluorescence from dye molecules above the bilayer (Figure 1C, D and Figure S2B).

Suspended Lipid Bilayers Are Unilamellar. In order to test whether single or multiple bilayers are resting on top of the cavities, we assayed pore formation by the bacterial toxin αHL. αHL is a water-soluble protein and binds as a monomer to choline-containing lipid headgroups.[10] At the lipid surface αHL oligomerizes and spontaneously inserts as a heptamer into the membrane, thereby forming a water-filled pore with a diameter of around 1.4 nm at its narrowest constriction.[11−14] Thus, small membrane-impermeable molecules such as the organic fluorophore Alexa Fluor 488 (MW 643 Da) can diffuse through the membrane-inserted αHL. Due to its large soluble domain, αHL cannot cross the membrane and forms a pore only through a single bilayer. To assay αHL pore formation, cavities were sealed by rupture of GUVs (lipid composition termed "endosomal mimic" consists of 80% phospholipids: 4.9/2/1.5/1.5/0.1/0.01 ratio of 1,2-dioleoyl-*sn*-glycero-3-phosphocholine (DOPC)/DOPE/1,2-dioleoyl-*sn*-glycero-3-phospho-L-serine (DOPS)/1,2-dioleoyl-*sn*-glycero-3-phospho-(1′-*rac*-glycerol) (DOPG)/disialoganglioside GD1a (GDa1)/Atto390-DOPE and 20% cholesterol) in the presence of the sealing-control fluorophore Oyster 647 (λ_{em} 673 nm, MW 1450). After washing of the chip, the entrapped red fluorophore serves to identify sealed cavities (Figure 1C and D). Alexa Fluor 488, added after GUV rupture, fills only cavities that are not well sealed by a lipid membrane; the sealed cavities remain dark (Figure 1D, t = 0). Addition of 0.5 μM αHL to the buffer reservoir above the chip led to a rapid increase of the Alexa Fluor 488 fluorescence in 98% of the sealed cavities, eventually reaching the fluorescence level of open, unsealed, cavities (Figure 1D, t = 7−14 min, and supplementary video SV1). This result demonstrates that a single lipid bilayer forms the seal on top of the cavities.

Assembly of αHL Is Dependent on the Ionic Strength. We repeated the experiment mentioned above using the "endosomal lipid mimic" but at higher ionic strength in order to investigate the influence of salt on αHL pore formation. To this end, chip hydration and GUV swelling and rupture were performed with buffer supplemented with 75 and 150 mM NaCl (190 and 340 mOsm/L), respectively. Remarkably, at increased ionic strength only a small fraction of the sealed cavities (9.7% at 75 mM and 4.7% at 150 mM NaCl supplement) displayed significant fluorescence increase upon αHL addition (Figure 2A and supplementary video SV2). Moreover, transport of Alexa Fluor 488 into individual cavities occurred at a 13−14-fold lower rate (Figure 2B). Likely, at optimal conditions at low ionic strength, the high pore formation efficiency resulted in insertion of multiple pores per bilayer patch spanning a single cavity (~0.85 μm in diameter), leading to increased transport rates. To determine the transport rate of a single αHL pore, we conducted the experiment at low ionic strength and 50 nM αHL (data not shown). At such low protein concentration only 0.8% of the sealed cavities showed transport, making it statistically unlikely that two pores were inserted in the same bilayer patch above a single cavity. The average rate constant determined from fitting the transport curves was $(2.55 \pm 1.04) \times 10^{-5}$ s^{-1} (~0.27 molecule s^{-1}), which is in good agreement with the rate constant for transport at high ionic strength and 0.5 μM αHL, and $(1.86 \pm 0.28) \times 10^{-5}$ s^{-1} (~0.2 molecule s^{-1}) and $(1.76 \pm 0.2) \times 10^{-5}$ s^{-1} (~0.19 molecule s^{-1}) for 75 and 150 mM NaCl, respectively. This indicates that also at these conditions a single αHL pore was inserted per cavity. The estimates for the number of molecules transported per second are obtained from the fluorescence intensity using the following reasoning: Bilayer-sealed cavities do not show any fluorescent signal in the presence of 10 μM fluorophore above the bilayer. Upon αHL pore formation, fluorophore molecules diffuse into the cavity below the bilayer until equilibrium is reached, observable as an asymptotic increase of fluorescence to the level of unsealed cavities (Figure 1D). With the volume of a cavity being equal to 6.5 fL, a concentration of 10 μM fluorophores translates to around 39 100 molecules per cavity at maximum fluorescence intensity. The exact detection volume inside the cavity is, however, unknown, and therefore the number of molecules transported is only an approximation.

Single-Channel Analysis Reveals Population Heterogeneity. Further support of the hypothesis that the observed fluorophore transport occurred through single αHL pores is provided by the distinct nature of the transition from the nonconducting to fluorophore transport state occurring often only after several hours' incubation with αHL at high ionic strength (Figure 2C). At 75 mM NaCl, the majority of cavities (69%, 292 cavities) with transport events displayed a regular fluorescence increase expected for import diffusion through a narrow pore (Figure 2C). The remaining 31% of curves, however, showed irregular behavior. In particular, for a significant number (13.1%, 55 cavities) transport was interrupted, marked by a sharp transition to the nonconducting state (Figure 2D). In most cases, transport was continued after some time. Perhaps, at higher ionic strength, αHL heptamers can disassemble more frequently, leading to a collapse of the pore. Formation of a new heptameric pore may then re-establish full conductance. Another group of irregular curves (6.9%) displayed a very slow conducting state prior to the transition to full fluorophore conductance, which is similar to rate constants of single pores at low ionic strength (Figure 2E). Rupture of the cavity-spanning membrane induced by αHL occurred especially at high ionic strength and was in most cases accompanied by migration of lipids into the cavities, as observed by

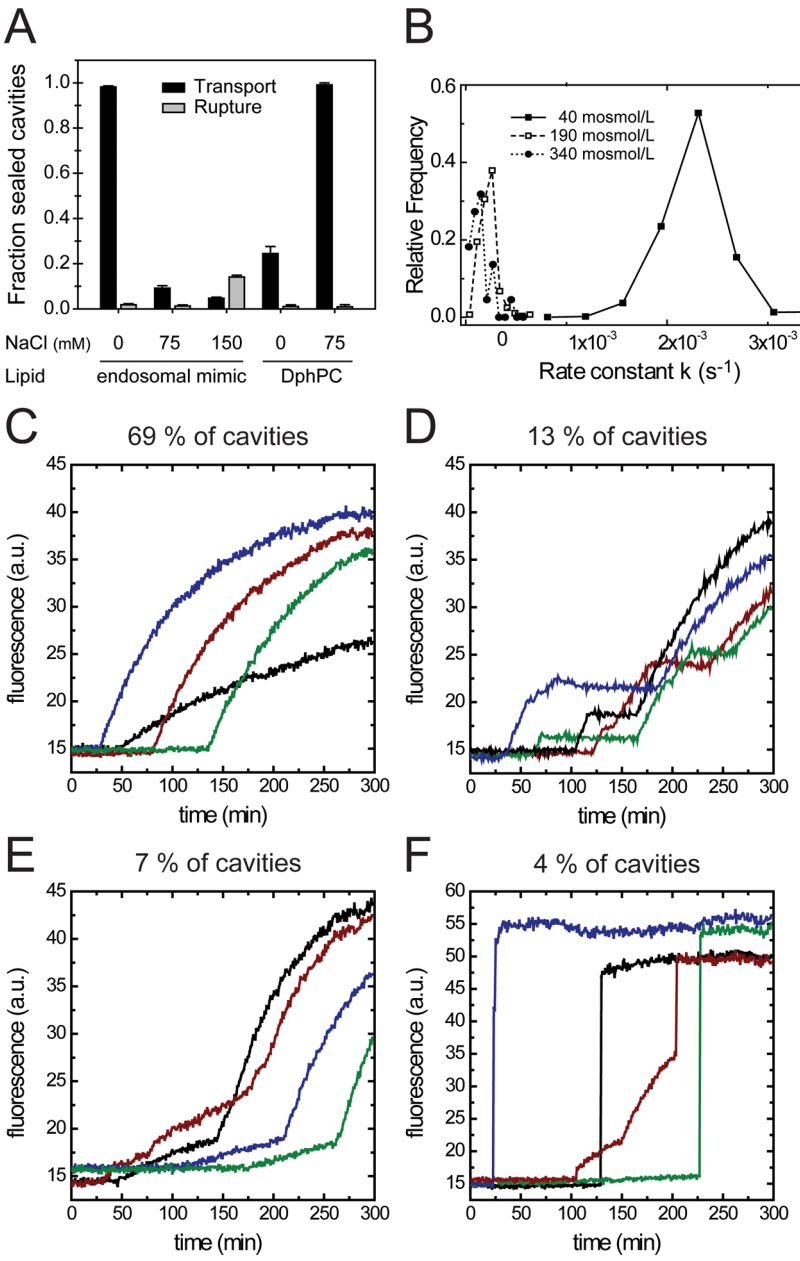

Figure 2. Single-channel kinetics reveal population heterogeneity. (A) Efficiency of αHL pore formation with respect to the ionic strength in a native lipid mimic and saturated lipid bilayer from DPhPC. Membrane rupture is detected by rapid increase of fluorescence or by migration of lipid into the cavities. Error bars are normalized sigma. (B) Rate constant distribution of αHL-mediated fluorophore import at various ionic strengths. (C−F) Examples of αHL transport events at 190 mOsm/L (75 mM NaCl supplement). (C) The majority of curves show regular import diffusion and distinct transition to conductance. (D) Interruption of transport occurs at high ionic strength. (E) A long-lasting low conducting state followed by transition to full conductance is observed in a subset of pores. (F) Membrane rupture is accompanied by rapid influx of fluorophores.

fluorescence of the embedded lipid marker Atto390-DOPE (Figure S3). For the transport substrate, membrane rupture resulted in an instantaneous fluorescence increase to maximum level (Figure 2F).

Ionic Strength Acts Contrariwise on αHL Insertion into Saturated Lipids. In previous studies, αHL insertion into planar bilayers composed of diphytanoyl-phosphatidylcholine (DPhPC) was studied at high ionic strength.[15−18] Thus, we investigated if the observed inhibition of αHL insertion by salt also occurs in lipids with branched saturated fatty acid chains such as DPhPC. Remarkably, salt had the opposite effect with such membranes as compared to lipids containing unsaturated oleic acids. At low ionic strength (40 mOsm/L) the insertion efficiency was only 24.5%, while in buffer supplemented with 75 mM NaCl (190 mOsm/L) 99.1% of sealed cavities showed transport (Figure 2A). Hence, the observed salt sensitivity of αHL pore formation appears to be connected with the nature of the acyl chain region of the membrane.

Taken together, these results demonstrate that single membrane transporter kinetics can be obtained

with hundreds of individual recordings in a single experiment using physiologically relevant lipid compositions and salt concentrations.

αHL Pore Formation and Fluorophore Conductance Is Dependent on the Lipid Composition. The lipid composition of the target membrane was previously shown to be important for binding and oligomerization of αHL.[10,19] Membrane binding and oligomerization of αHL is dependent on the choline group of phospholipids and sphingomyeline.[19−21] The lipid dependence of αHL pore formation as well as conductance of αHL pores embedded in different lipid environments has not been quantitatively addressed so far due to the technical challenge of measuring membrane transport with single-pore resolution. In traditional vesicle efflux assays pore-forming efficiency and fluorophore conductance of individual pores are merged and population heterogeneity is averaged out. Hence, we investigated the αHL insertion efficiency and transport kinetics in different lipid mixtures. In particular, we investigated lipid mixtures with and without cholesterol and anionic lipids. We generated suspended lipid bilayers of the following four compositions: 7.9/2/0.1 DOPC/DOPE/GDa1 and 4.9/2/1.5/1.5/0.1 DOPC/DOPE/DOPS/DOPG/GDa1 both as only phospholipids or an 8/2 phospholipid/cholesterol mixture.

In the absence of both negatively charged lipids and cholesterol, αHL inserted only in 31% (336) of sealed cavities (1086) (Figure 3A). When either cholesterol or negatively charged lipids were present in the membrane, pore formation efficiency almost doubled; 58.9% (269 of 457 cavities) in the presence of cholesterol and 61% (735 of 1205 cavities) in the presence of DOPS/DOPG. Interestingly, the positive effect of both lipid types added up to 75.3% (831 of 1103 cavities) insertion efficiency when both were present, suggesting that these lipid species promote αHL pore formation in two independent ways (Figure 3A). For each of these data sets, several hundred cavities were analyzed (Figure 3A). The rate constants of all regular αHL transport events were obtained by fitting import curves with single exponentials. The distribution of rate constants of αHL in membranes void of cholesterol and anionic lipids clearly shows that distinct subpopulations of pores exist with significantly different transport rates (Figure 3B).

Comparison with Bulk Assays. In previously employed ensemble assays, different rates of fluorophore leakage out of the liposome could originate from changes in pore formation efficiency or fluorophore conductance of individual αHL pores or both. Hence, in order to compare the here-obtained results with previous studies, the average rate constant of all individual transport events was determined displaying a large error, invisible in bulk measurements (Figure 3C). To estimate transport rates as observed in liposome leakage assays, the product of pore formation efficiency and average transport rate constant ($E \times k$) was calculated for all lipid mixtures (Figure 3D). Overall, cholesterol stimulates αHL-induced transport more strongly than anionic phospholipids, consistent with earlier studies.[10,22] However, since in bulk assays also interrupted or irregular transport events are counted, which in our data set could not be fitted accurately, this comparison can serve only as an estimate.

Simulating a Drug Screening Approach for Therapeutic Antibodies. During severe infections of *Staphylococcus aureus*, patients receive antibodies against αHL to reduce cell damage and nutrition availability. To simulate the search for new therapeutic antibodies against pore-forming bacterial toxins or membrane-penetrating viruses, we tested polyclonal antibodies raised in rabbits against αHL and unrelated antibodies raised against the bacterial protein YajC as a control. We generated suspended bilayers from porcine brain polar lipid extract supplemented with 20% cholesterol as a natural membrane substrate for αHL. First, the stability of the bilayer was tested in the presence of 0.5 μM of the antibodies. No membrane rupture occurred within 25 min, demonstrating that the antibodies can be used in combination with suspended bilayers (Figure 3C). Addition of 1 μM αHL resulted in pore formation for all bilayer patches incubated with the anti-YajC antibody, while no pores occurred in the presence of anti-αHL antibody. These data show that a stable suspended bilayer from native lipid extracts can be formed and that microporous silicon chips can be used in screening therapeutic antibodies raised against membrane targets.

Specialized Chip Architecture for Direct Visualization of Viral Membrane Fusion. Many pathogenic viruses such as influenza or corona viruses are surrounded by a lipid bilayer that functions as a transport vehicle to infect cells. The nucleic acid and proteins of the virus interior are injected into the cell when the viral and target membranes fuse during the infection cycle. Influenza viruses are taken up into the cell *via* endocytosis, and acidification of the endosomes triggers fusion of viral and endosomal membranes. To mediate adhesion to target cells and membrane fusion, specialized proteins are embedded in the virus envelope. Suspended lipid bilayers would be ideal to study the dynamics of membrane fusion and content release as well as to screen for drugs or therapeutic antibodies against membrane-penetrating viruses. Because with the above used nanoFAST E800 chips the membrane, resting on top of the cavities, is not visible from below, a different chip type, termed nanoFAST C800, was tested. The diameter of the cavities of this chip is wider (4 μm with a center-to-center distance of 8 μm), allowing illumination light from below to reach the suspended membrane. For the generation of stable bilayers, the cavities are topped by a glass lid with apertures of 1 μm (Figure 4A and B). In this configuration

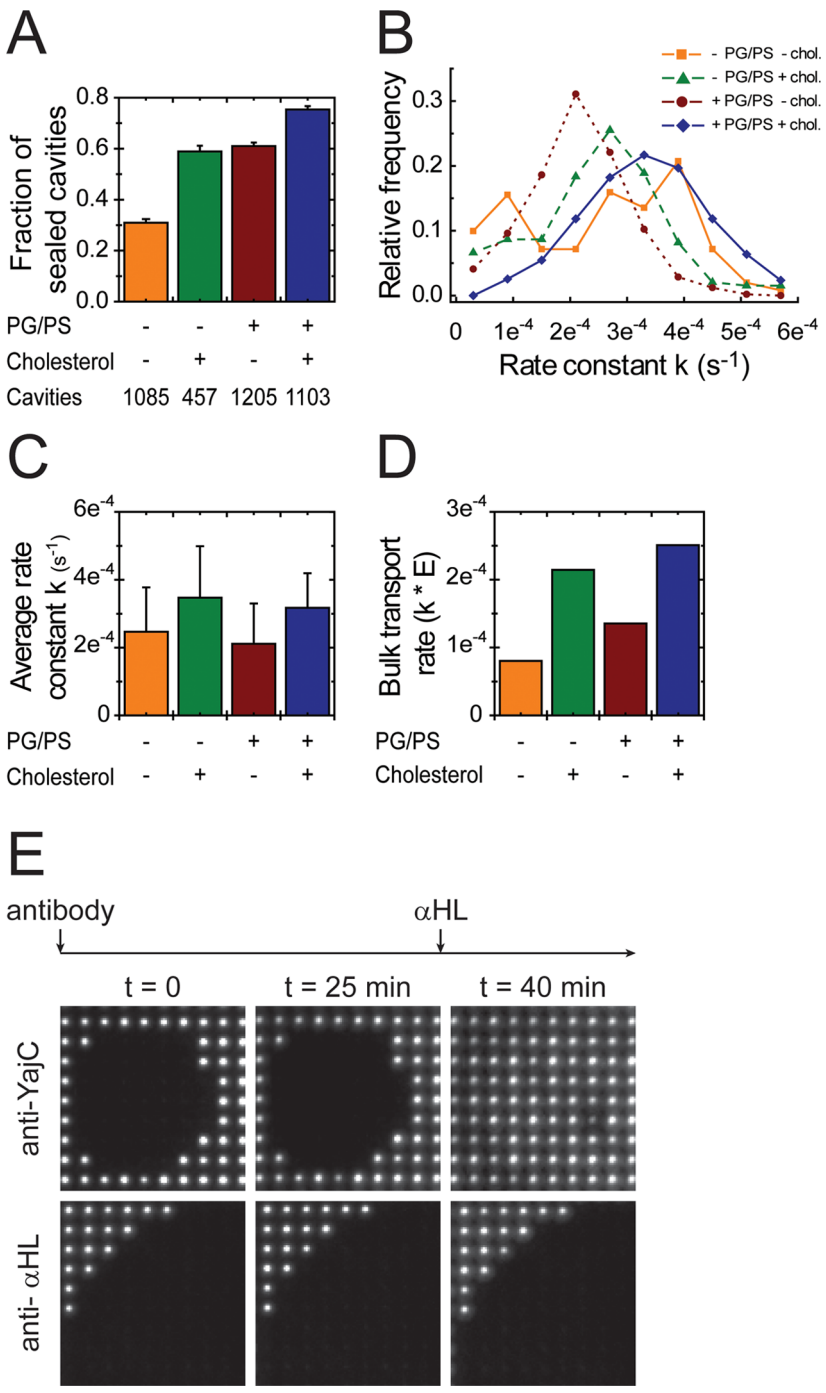

Figure 3. Hemolysin pore formation efficiency and conductance in different lipid compositions and in the presence of antibodies. (A) αHL pore formation efficiency in the presence or absence of anionc lipids and cholesterol, respectively. Both cholesterol and negatively charged lipids promote αHL insertion. Number of analyzed cavities is indicated. Error bars are normalized sigma. (B) Rate constant distributions of αHL pores inserted in indicated lipid compositions. Subpopulations of pores conduct differently in the absence of cholesterol and anionic lipids. (C) Average rate constants of αHL-induced transport as calculated from B. Error bars are standard deviation. (D) For comparison with bulk measurements, a bulk transport rate can be estimated from the product of insertion efficiencies and average rate constants. (E) Suspended bilayers composed of polar lipid extract from porcine brain supplemented with 20% cholesterol are stable in the presence of IgGs. A polyclonal antibody against αHL prevents pore formation, while a nonspecific antibody has no effect.

both glass-supported and free-standing bilayers are visible, while with the available gold layer only the suspended part of the bilayer is seen (Figure S4).

Membrane Fusion on Chip. Viral membrane fusion can be detected by introducing a lipid dye such as DiD into the viral envelope.[23−25] DiD spontaneously inserts into lipid bilayers in self-quenching concentrations. Upon membrane fusion, DiD will diffuse laterally into the target membrane, resulting in a dequenching signal followed by dissipation of the fluorescence

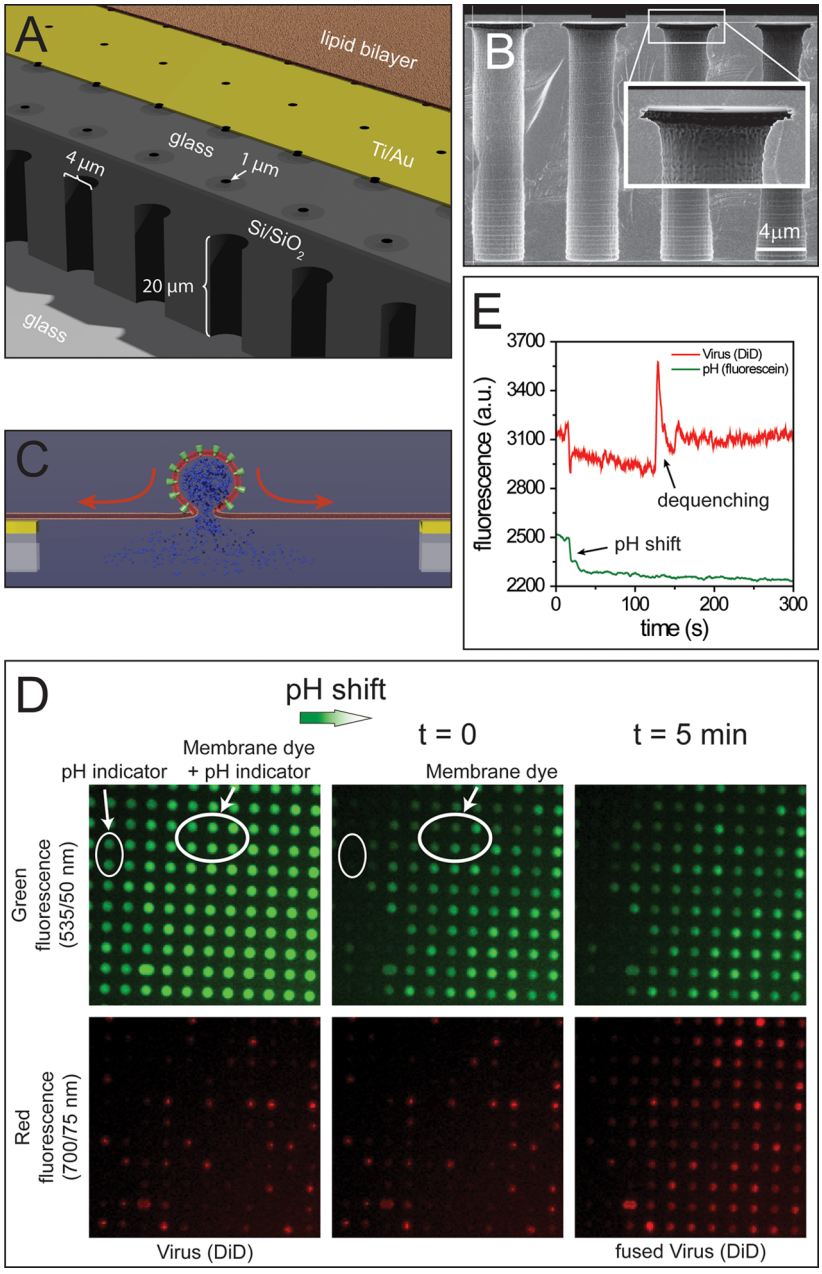

Figure 4. Direct observation of viral membrane fusion of influenza H3N2 on a NanoFAST C800 chip. (A) Specialized chip (C800) for monitoring processes at or in membranes (the different layers of the chips are shifted backward to illustrate the structure). Wide cavities allow light transmittance and are topped by a glass lid with smaller apertures to enable formation of a stable suspended bilayer. An optional gold layer facilitates surface modifications. Only suspended bilayers are visible with an additional Ti/Au layer (Figure S4). (B) Electron microscopy image of a NanoFAST C800 chip. The glass lid on top of the 4 × 20 μm cylindrical cavities has an aperture of ~1 μm (inset). (C) Influenza virus labeled with DiD bound to suspended bilayer. Upon fusion, the membrane dye DiD diffuses into the target membrane, leading to a dequenching signal. (D) Dual color imaging of chip-immobilized membrane (green lipid dye Bodipy-FL and carboxyfluorescein, upper panel) and bound H3N2 influenza viruses (red lipid dye DiD, lower panel). Fluorescence of the pH indicator dye fluorescein is quenched after acidification of the buffer. Viral membrane fusion leads to diffusion of DiD into the entire suspended and supported lipid bilayer patch (lower panel t = 5 min). Variations in green fluorescence are due to the illumination profile. (E) Direct observation of single viral membrane fusion events. Fusion occurs after acidification and is detected by fluorescence dequenching of DiD.

(Figure 4C and E). To test viral fusion with physiologically relevant membranes, a lipid mixture mimicking the composition of late endosomes,[26] the target membrane of influenza viruses, was used to form GUVs at physiological ionic strength (80% phospholipids: 4.9/2/1.5/1.5/0.1/0.00025 ratio of DOPC/DOPE/DOPS/DOPG/GDa1/Bodipy-FL and 20% cholesterol).

Due to the optical feature of the chip, the embedded green membrane dye Bodipy-FL is visible in the deposited bilayer (Figure 4D, upper panel).

Acidification is the trigger for membrane fusion mediated by the viral protein hemagglutinin and is realized by addition of buffer containing citric acid, which leads to lowering of the pH to 5. As an indicator of acidification, the pH-sensitive fluorophore carboxyfluorescein was added to the buffer. As carboxyfluorescein and Bodipy-FL have similar emission spectra, first suspended membranes were identified by Bodipy-FL fluorescence followed by fluorescein addition, which masked the emission of the membrane dye (Figure 4D, upper panel). After acidification, fluorescein emission is highly quenched, allowing the exact temporal assignment of the pH shift (Figure 4D and E). Influenza H3N2 viruses labeled with DiD bind to the disialoganglioside receptor and remain membrane bound after washing, as seen by fluorescence in the red channel (Figure 4D, lower panel). Membrane fusion of individual viruses following acidification is detected by characteristic dequenching signals of DiD in the red channel (Figure 4D). Since the membrane dye DiD diffuses into the target membrane, the entire bilayer patch is visible in the red channel (Figure 4C; compare green and red fluorescence at $t = 5$ min). Lateral mobility of the lipids in a supported and suspended bilayer was confirmed by fluorescence recovery after photobleaching of DiD after virus fusion (Figure S5). These data demonstrate that suspended lipid bilayers composed of physiologically relevant lipids can be used to study the dynamics of membrane fusion.

DISCUSSION

Here we present the next generation of microstructured chips that are evolved to a state that high-throughput analysis of membrane transport events as well as membrane fusion and drug screening against membrane targets are feasible. To this end, rupture of GUVs was used to form unilamellar suspended bilayers spanning microporous cavities. Thanks to recent advancements of GUV preparation by gel-assisted swelling of dried lipid films, complex lipid mixtures including cholesterol and native extracts can be converted to GUVs at high ionic strength.[7,8] We also find these protocols superior to the traditional electroformation technique due to the ease and speed of preparation. A previous bottleneck in producing GUVs with embedded membrane proteins is under constant progress, as several strategies were described to reconstitute membrane proteins into preformed GUVs[27−29] that could also be combined with the efficient gel-assisted swelling. Alternatively, membrane proteins can be incorporated prior to GUV formation,[30,31] or GUVs can be generated directly from native membranes.[32,33] Hence, the study of a membrane transporter embedded in suspended lipid bilayers that require GUV formation is well feasible. Suspended bilayers further have the advantage that inserted membrane proteins or peptides are not in contact with the solid support, which often leads to immobilization and subsequent inactivation of the proteins. Membrane proteins immobilized on the solid support between the suspended bilayer patches will not participate in transport processes into the cavities of the chip. Although GUV rupture on solid surfaces was shown earlier to result in a single rather than two stacked lipid bilayers,[34−36] we confirmed the existence of unilamellar membranes by insertion of the bacterial toxin αHL, which can penetrate only a single bilayer due to its large hydrophilic domain. Hemolysins and other bacterial toxins are secreted by pathogenic bacteria to kill host cells in order to scavenge nutrients.[37] αHL is a water-soluble protein that binds as a monomer to cell surface receptors, in particular to the choline group of phospholipids.[10,20,21] Oligomerization occurs in the membrane-bound state, leading to the formation of the intermediately heptameric prepore,[12,38−40] which spontaneously inserts into the lipid bilayer, forming a water-filled channel.[14] Despite the multitude of studies on pore formation by bacterial toxins, the mechanism of pore assembly of αHL is poorly understood. In particular, the interplay between lipid headgroups and the hydrophobic core of the membrane with the polypeptide as well as their role in oligomerization and insertion is intensively researched.[10,19−21,41,42] Two methodologies are commonly employed to address αHL activity: fluorophore leakage from liposomes upon pore formation and ion conductance measurements in planar lipid bilayers. While liposome leakage assays can be performed with any desired lipid composition, important kinetic parameters such as timing of pore formation, number of pores, and individual pore conductance are concealed in the bulk measurement.[43] Electrophysiological experiments enable recordings of single pores with high temporal resolution but suffer from the fact that mostly nonphysiological lipid bilayers with high electrical resistance are studied. Thus, the majority of electric recordings of single αHL pores were done using the lipid diphytanoylphosphatidylcholine.[15−17,44] New technologies employing parallel electrical recording across artificial bilayers are emerging, but deposition of suspended bilayers usually involves organic solvents that are harmful to inserted membrane proteins.[45,46] Furthermore, parallel electrical readout of thousands of individual bilayer patches is very challenging but may eventually provide high temporal resolution of transport processes.

To demonstrate high-throughput analysis of a medically relevant membrane channel, we studied αHL pore formation and its dependence on lipid environment and ionic strength. Surprisingly, we found efficiency of αHL pore formation to be strongly reduced at physiological ionic strength, which is in contrast to previous studies.[15−18] A major difference in our initial experiments was the lipid composition, which was designed to mimic the plasma membrane

of mammalian cells, thus containing mainly unsaturated lipids. αHL transport assays with DPhPC, a lipid with branched saturated fatty acids, as used in the other studies revealed that pore formation by αHL was more efficient at high ionic strength, which is consistent with previous results. We speculate that saturated lipids may promote αHL insertion into the membrane or stabilize the heptameric form against disassembly. Single-channel analysis of αHL fluorophore conductance in the plasma membrane mimic at unfavorable high ionic strength reveals population heterogeneity of pore conductance. While the majority of transport events follow regular import kinetics, a significant fraction of the pores shows either very slow conductance or interrupted transport. The sharp transitions to the import stop were previously interpreted by diffusion of membrane pores out of the suspended bilayer into the solid-supported bilayer part next to the cavities.[4] However, at low ionic strength or other conditions with low insertion efficiency we did not observe such interrupted transport signatures, and in the previous study the experiments were performed only at high ionic strength. Instability or even disassembly of αHL heptamers has not been described so far, but single-channel recordings of αHL were previously conducted only at favorable insertion conditions. Here, this indeed also resulted only in homogeneous transport curves. Further studies are required to investigate the oligomerization of αHL and the stability of the heptamer at physiological conditions.

Assembly rates, *i.e.*, the time from addition of αHL to the suspended bilayers until the observation of a conducting state, were not quantitatively analyzed in this study. Apparently at unfavorable conditions more pores occur at later time. The rate constants derived from "regular" import curves of single pores at different ionic strengths were, however, similar, once they occurred.

An intensively researched topic in the field of bacterial toxins is the lipid dependence of pore assembly (for review see ref 42). Previously, strong stimulation of αHL pore formation by cholesterol was shown,[10,22] but due to the liposome leakage assay employed in these studies, the discrimination between enhanced insertion efficiency leading to a greater number of pores and higher conductance of individual αHL channels could not be made. By investigating αHL transport with single-pore resolution across membranes with controlled lipid composition we show not only that the insertion efficiency is promoted by the presence of cholesterol and anionic phospholipids but that also a subpopulation of low-conducting αHL pores exist in membranes lacking cholesterol. Thus, the observed stimulation of αHL activity by cholesterol appears to rely on both increased number of pores and performance of individual pores. Possibly, cholesterol and anionic lipids stabilize the heptameric form or facilitate conversion of the prepore to the fully conducting state, a hypothesis that could be studied with fluorescently labeled αHL subunits and supported lipid bilayers.[44,47] Alternatively, binding of the αHL monomers to the membrane could be enhanced by interaction of the polypeptide with anionic headgroups and the hydrophobic core of the lipid bilayer.[19,20] Due to the slow diffusion of fluorophores through αHL pores, only one image with a 100 ms exposure time was taken once a minute. The acquisition settings are easily adapted for faster transporters with a possible time resolution of tens of milliseconds, but this also depends on the sensitivity of the CCD camera and the objective used.

Taken together, we measured membrane transport across lipid bilayers composed of physiologically relevant lipid compositions and at physiologically relevant salt concentrations. Studying αHL assembly with single-pore resolution reveals the population heterogeneity of pore assembly and conductance at physiological conditions.

In previous studies, a proof-of-principle was provided that suspended lipid bilayers can be formed resting on nano- or microporous substrates.[4−6] Kleefen *et al*. showed that membrane pores can be incorporated into the suspended membranes and efflux of an entrapped fluorophore could be visualized as an escaped fluorophore diffused into the large buffer volume above the chip. The here-presented microporous chips have substantial advantages over previously described chip designs. While continuous imaging of entrapped fluorescent substrates for efflux experiments is prone to photobleaching,[4] imaging of import is more sensitive due to the higher signal-to-background ratio. Furthermore, in contrast to chips that require dipping of the objective into the fluorophore-containing buffer above the chip, fluorescent readout with the here-presented chips occurs with air objectives from below, allowing fast measurements of multiple chips. The yet poorly understood phenomenon that the microcavities transmit almost no excitation light or fluorescence from above the chip allows the unambiguous optical separation of the cis- and trans-side of the suspended membrane. Possibly, the 10 μm deep cylindrical cavities are not well enough aligned to the optical axis of the microscopes and light is scattered at the pore walls. Thus, only fluorescent molecules inside the cavities are detected. Microstructured silicon chips were previously used to observe migration of fluorescently labeled cell-penetrating peptides into cavities sealed by lipid bilayers.[48] Unfortunately, only average penetration rates were calculated from the distribution of multiple migration events, yielding information similar to bulk experiments. Yet, the possibility to obtain distributions of membrane transport across individual membrane patches is a powerful tool to discover population heterogeneity and single-transporter kinetics.

Fusion of viruses with their target membrane is the key to the penetration of cells and propagation of the infection. Hence, the mechanism of viral membrane fusion is of great scientific and medical interest. Suspended lipid bilayers as presented here are an ideal tool to study the dynamics and lipid dependence of membrane fusion as well as inhibition by antibodies or drugs. Screening for new therapeutic antibodies that requires high-throughput analysis is thus a potential application of the here-presented chips especially as antibodies do not interfere with the integrity of the suspended bilayers. Previously, polymer-cushioned lipid bilayers and microfluidics were used to study viral fusion and content release, but this technique requires sophisticated and time-consuming surface modification and sample preparation, taking several days prior to the experiment. Furthermore, only neutral lipids are used to form the cushioned bilayers, limiting the simulation of biological target membranes. Microstructured Si/SiO_2 chips offer the advantage of fast sample preparation and generation of suspended membranes of physiologically relevant lipid composition that allow the study of both hemifusion and content release.

CONCLUSIONS

The here-presented technology presents several advantages over traditional approaches to study membrane transport. First, any lipid mixture that is capable of forming GUVs can be used to seal microcavities structured in Si/SiO_2 chips with unilamellar lipid bilayers. Stability of the suspended membranes exceeds by far the experimental requirements to study biological processes. Second, except for the C800-gold chip, no surface modification or sophisticated sample preparation is required, and the entire protocol for generation of suspended bilayers can be done in less than three hours. Third, membrane transport can be studied at various salt concentrations, allowing the controlled simulation of physiological conditions, unlike electrophysiological recordings, which require high concentrations of ions and lipids that constitute bilayers with high electrical resistance. Fourth, the spatial separation of the microcavities allows simultaneous observation of hundreds of individual membrane transporters. This is especially of interest when population heterogeneity, kinetic parameters, and number of active transporters are of interest.

METHODS

Reagents. NanoFAST E800 and C800 biochips were obtained from Nanospot GmbH, Münster, Germany. Lipids were purchased from Avanti Polar Lipids, except Disialoganglioside GD1a from bovine brain, which was from Sigma-Aldrich. Fluorescently labeled lipids were from Atto-Tec. Superlow melting agarose (HP45.1) for GUV formation was obtained from Carl-Roth, and polyvinyl alcohol (PVA) MW 145000 was from Merck (VWR). Cell-saver MidiTips for GUV pipetting were from Biozym. α-Hemolysin from *Staphylococcus aureus* and Pluronic F-127 were purchased from Sigma-Aldrich. Oyster fluorophores were from Luminartis GmbH, Alexa Fluor 488 NHS-ester and DiD were from Life Technologies, and 5(6)-carboxyfluorescein and dextran, 6 kDa (31388), were from Sigma-Aldrich. The PD MiniTrap G-25 column was from GE Healtcare, slide tray plates were obtained from Zell-Kontakt, and Con-Sil (component A: CON-SIL 12, component B: 116584 Bluestar Cata 24 H) was purchased from Polychem Handelsges.m.b.H., Austria.

GUV Formation. Two recently described protocols for GUV formation by gel-assisted swelling of dried lipid film were used in this study. Agarose-assisted swelling by Horger *et al.* allows formation of GUVs with high ionic strength buffers from all lipid mixtures used except DPhPC.[7] An advantage of this method is the high yield and size of the GUVs (20−50 μm for high ionic strength and lipid mixtures without anionic lipids; 50−100 μm for low ionic strength and lipid mixtures including anionic lipids). The related approach by Weinberger *et al.* allows the generation of GUVs without contamination of polymers as well as at higher temperature.[8] With this method, the yield of GUVs from less stable lipid mixtures such as brain polar lipid extract is higher, possibly because of milder harvest conditions, as the GUVs form on top of a stable hydrogel, which does not detach from the glass surface. In both methods, GUVs are generated by swelling of a dried lipid film deposited on a microscope glass slide coated with a dried hydrogel. First, standard microscope slides (75 × 25 × 1 mm) were cleaned with 2-propanol and acetone either by placing them in a jar and bath sonicator for 20 min or by rubbing them with lint-free paper and the solvent. The slides were rinsed with copious amounts of demineralized water, blown dry, and placed on a heating plate set to 50 °C. Then 200 μL of 1% (w/v) superlow melting agarose or 300 μL of 5% (w/v) PVA heated to 50 °C prior to use was pipetted on the slide and spread out using a glass stick or pipet until it became viscous. The resulting agarose or PVA film was dried for 30 min on the heating plate or placed in a Petri dish in an oven at 55 °C. Lipids were dissolved in chloroform to 4 mg/mL, and 30 μL was spread on each of the halves of the agarose-coated slide using a glass Pasteur pipet. In order to keep the 300 μL swelling buffer (20 mM Hepes-KOH pH 7.5 supplemented with up to 150 mM NaCl and 1 mg/mL dextran) in place, silicon rings of 2 cm diameter were cut from sheets of Con-Sil and stuck to the glass slide prior to swelling. Con-Sil sheets of 1−2 mm thickness can be generated by casting a mixture of components A and B (20:1 ratio) into a Petri dish followed by curing at RT for 24 h. Incubation of the GUV swelling reaction at RT for 30 min to 2 h was sufficient to generate GUVs for all lipid mixtures. Detachment of the GUVs from the surface was facilitated by gently swinging the glass slides followed by harvesting with a pipet equipped with cell saver tips. GUVs were stored at RT in Protein LoBind Eppendorf tubes until use and for a maximum of 24 h. GUVs from DPhPC were formed by electroformation in 1 mg/mL dextran in dH_2O with the following settings: 10 Hz frequency, amplitude 0−1.5 (start−end), 150 steps for 120 min followed by 22 h at amplitude 1.5.

Generation of Free-Standing Lipid Bilayer on NanoFAST E800 and C800 Chips. NanoFAST (fluorescence analysis of single transporters) E800 chips are provided from Nanospot GmbH precleaned in eight-well sample holders, and fresh chips were used without further cleaning. Each well has the dimensions 9.4 × 10.7 × 6.8 mm (w × l × h), and a minimum volume of 250 μL is required to cover the chip, while the maximum volume for washing is 800 μL. Chips stored at ambient conditions for more than two weeks were reactivated in a 100 mA oxygen-plasma cleaner for 2 min. This step is not always necessary but may improve formation of suspended bilayers. Wells containing NanoFAST E800 chips and 250 μL of buffer (20 mM Hepes-KOH pH 7.5 supplemented with up to 150 mM NaCl, 0.5 mM $CaCl_2$, or 1 mM $MgCl_2$ to mediate surface attachment of the GUVs and 1−10 μM sealing-control

fluorophore to identify sealed areas) were sonicated for 20 s in a bath sonicator to remove air bubbles trapped in the cavities. Wells of the sonication-incompatible NanoFAST C800 chips were first filled with 300 μL of ethanol and incubated for 5 min on a nutating mixer to exclude air. Ethanol was removed by washing the wells five times with 500 μL of demineralized water followed by five washing steps with the desired buffer containing 0.5 mM $CaCl_2$. Dependent on the GUV yield, 10−30 μL of GUVs, generated in buffer of the same ionic strength as the buffer around the chip with addition of 1 mg/mL dextran, was pipetted into the well. The eight-well holder was placed in a slide tray plate that functioned as an adaptor for the 96-well plate carrier of a swing-out centrifuge. GUVs were ruptured by 5 min centrifugation at 100*g*.

Surface Modification of NanoFAST C800-Gold Chips. To facilitate GUV rupture on the gold surface, nanoFAST C800-gold chips were coated with a self-assembled monolayer of 3-mercaptopropionic acid (MPA). After 2 min treatment in a 100 mA oxygen-plasma cleaner, air was removed from the cavities by ethanol washing as described above for the C800 chips followed by five wash steps with demineralized water and five wash steps with 5 mM MPA in water. After 1 h incubation at RT, unbound MPA was removed by five wash steps of each demineralized water and buffer, respectively. GUV attachment to the anionic surface and subsequent rupture were mediated by 0.5 mM $CaCl_2$ in the buffer as for the C800 and E800 chips.

Fluorescent Labeling of Influenza H3N2 Viruses. Membrane staining of influenza H3N2 viruses (strain X31) with DiD was done as described previously.[24,25] In short, 15 μL of a virus suspension containing 2 mg/mL total protein was diluted with 45 μL of HNE buffer (10 mM Hepes-KOH pH 7.5, 140 mM NaCl, 0.2 mM EDTA) and mixed with 1 μL of 1 mM DiD in DMSO supplemented with 1% Pluronic F-127 to help disperse DiD micelles. After 30 min incubation at RT, unincorporated DiD was removed by purifying the viruses *via* a PD MiniTrap G-25 column equilibrated in HNE buffer.

Light Microscopy and Data Analysis. Fluorescence readout of the chips was performed with bright field fluorescence microscopes equipped with air objectives (20× or 40×). Experiments were done on a commercial NyOne automated fluorescence microscope (SynenTec BioServices GmbH, Germany) equipped with LED light sources (excitation filters 377/50, 475/28, 632/22 nm), an Olympus UPlan SApo 20×/0.75 objective, and a 1.45 megapixel CCD-camera and on a home-built inverted fluorescence microscope (Olympus IX-71) equipped with 488, 532, and 641 nm lasers, an Olympus LUCPLFLN 40XPH objective, a DualView2 beam splitter/emission filter module, and an EM-CCD camera (512 × 512 pixels, Hamamatsu Photonics). Image analysis (drift correction, identification of fluorescent areas, and extraction of time series) was done with ImageJ and freely available plugins: template matching (https://sites.google.com/site/qingzongtseng/template-matching-ij-plugin) and time series analyzer (http://rsbweb.nih.gov/ij/plugins/time-series.html). Time series correlation and curve fitting were done with the open source data evaluation software NanocalcFX (from Nanospot). SEM pictures were provided by Nanospot.

Conflict of Interest: The authors declare no competing financial interest.

Acknowledgment. We would like to thank M. Vor der Brüggen (Nanospot GmbH) for the technical support. This research has been carried out with support from The Netherlands Organization for Scientific Research (NWO) and the Dutch Foundation for Fundamental Research on Matter (FOM).

Supporting Information Available: Phase contrast images of GUV rupture on microstructured Si/SiO_2, suspended bilayers on NanoFAST E800 imaged from top and stability of the bilayer seal, αHL-induced membrane rupture at high ionic strength, imaging of unilamellar suspended lipid bilayer on C800-gold chips, fluorescence recovery after photobleaching (FRAP) after viral membrane fusion. Videos of αHL hemolysin mediated fluorophore influx into cavities of a NanoFAST E800 chip at low and high ionic strength, respectively. This material is available free of charge *via* the Internet at http://pubs.acs.org.

REFERENCES AND NOTES

1. Bakheet, T. M.; Doig, A. J. Properties and Identification of Human Protein Drug Targets. *Bioinformatics* **2009**, *25*, 451–457.
2. Tamm, L. K.; McConnell, H. M. Supported Phospholipid Bilayers. *Biophys. J.* **1985**, *47*, 105–113.
3. Tanaka, M.; Sackmann, E. Polymer-Supported Membranes as Models of the Cell Surface. *Nature* **2005**, *437*, 656–663.
4. Kleefen, A.; Pedone, D.; Grunwald, C.; Wei, R.; Firnkes, M.; Abstreiter, G.; Rant, U.; Tampé, R. Multiplexed Parallel Single Transport Recordings on Nanopore Arrays. *Nano Lett.* **2010**, 1–9.
5. Lazzara, T. D.; Carnarius, C.; Kocun, M.; Janshoff, A.; Steinem, C. Separating Attoliter-Sized Compartments Using Fluid Pore-Spanning Lipid Bilayers. *ACS Nano* **2011**, *5*, 6935–6944.
6. Kocun, M.; Lazzara, T. D.; Steinem, C.; Janshoff, A. Preparation of Solvent-Free, Pore-Spanning Lipid Bilayers: Modeling the Low Tension of Plasma Membranes. *Langmuir* **2011**, *27*, 7672–7680.
7. Horger, K. S.; Estes, D. J.; Capone, R.; Mayer, M. Films of Agarose Enable Rapid Formation of Giant Liposomes in Solutions of Physiologic Ionic Strength. *J. Am. Chem. Soc.* **2009**, *131*, 1810–1819.
8. Weinberger, A.; Tsai, F.-C.; Koenderink, G. H.; Schmidt, T. F.; Itri, R.; Meier, W.; Schmatko, T.; Schröder, A.; Marques, C. Gel-Assisted Formation of Giant Unilamellar Vesicles. *Biophys. J.* **2013**, *105*, 154–164.
9. Danos, L.; Greef, R.; Markvart, T. Efficient Fluorescence Quenching near Crystalline Silicon from Langmuir−Blodgett Dye Films. *Thin Solid Films* **2008**, *516*, 7251–7255.
10. Watanabe, M.; Tomita, T.; Yasuda, T. Membrane-Damaging Action of Staphylococcal Alpha-Toxin on Phospholipid-Cholesterol Liposomes. *Biochim. Biophys. Acta* **1987**, *898*, 257–265.
11. Gouaux, J. E.; Braha, O.; Hobaugh, M. R.; Song, L.; Cheley, S.; Shustak, C.; Bayley, H. Subunit Stoichiometry of Staphylococcal Alpha-Hemolysin in Crystals and on Membranes: A Heptameric Transmembrane Pore. *Proc. Natl. Acad. Sci. U.S.A.* **1994**, *91*, 12828–12831.
12. Fang, Y.; Cheley, S.; Bayley, H.; Yang, J. The Heptameric Prepore of a Staphylococcal Alpha-Hemolysin Mutant in Lipid Bilayers Imaged by Atomic Force Microscopy. *Biochemistry* **1997**, *36*, 9518–9522.
13. Jayasinghe, L.; Miles, G.; Bayley, H. Role of the Amino Latch of Staphylococcal Alpha-Hemolysin in Pore Formation: A Co-Operative Interaction between the N Terminus and Position 217. *J. Biol. Chem.* **2006**, *281*, 2195–2204.
14. Song, L.; Hobaugh, M. R.; Shustak, C.; Cheley, S.; Bayley, H.; Gouaux, J. E. Structure of Staphylococcal Alpha-Hemolysin, a Heptameric Transmembrane Pore. *Science* **1996**, *274*, 1859–1866.
15. Korchev, Y. E.; Bashford, C. L.; Alder, G. M.; Kasianowicz, J. J.; Pasternak, C. A. Low Conductance States of a Single Ion Channel Are Not "Closed". **1995**, *239*, 233−239.
16. Gu, L. Q.; Braha, O.; Conlan, S.; Cheley, S.; Bayley, H. Stochastic Sensing of Organic Analytes by a Pore-Forming Protein Containing a Molecular Adapter. *Nature* **1999**, *398*, 686–690.
17. Karginov, V. A.; Nestorovich, E. M.; Schmidtmann, F.; Robinson, T. M.; Yohannes, A.; Fahmi, N. E.; Bezrukov, S. M.; Hecht, S. M. Inhibition of S. Aureus Alpha-Hemolysin and B. Anthracis Lethal Toxin by Beta-Cyclodextrin Derivatives. *Bioorg. Med. Chem.* **2007**, *15*, 5424–5431.
18. Oukhaled, G.; Bacri, L.; Mathé, J.; Pelta, J.; Auvray, L. Effect of Screening on the Transport of Polyelectrolytes through Nanopores. *EPL (Europhys. Lett.)* **2008**, *82*, 48003.
19. Schwiering, M.; Brack, A.; Stork, R.; Hellmann, N. Lipid and Phase Specificity of A-Toxin from S. Aureus. *Biochim. Biophys. Acta* **2013**, *1828*, 1962–1972.
20. Galdiero, S.; Gouaux, E. High Resolution Crystallographic Studies of Alpha-Hemolysin-Phospholipid Complexes Define Heptamer-Lipid Head Group Interactions: Implication for Understanding Protein-Lipid Interactions. *Protein Sci.* **2004**, *13*, 1503–1511.

21. Valeva, A.; Hellmann, N.; Walev, I.; Strand, D.; Plate, M.; Boukhallouk, F.; Brack, A.; Hanada, K.; Decker, H.; Bhakdi, S. Evidence That Clustered Phosphocholine Head Groups Serve as Sites for Binding and Assembly of an Oligomeric Protein Pore. *J. Biol. Chem.* **2006**, *281*, 26014–26021.
22. Forti, S.; Menestrina, G. Staphylococcal Alpha-Toxin Increases the Permeability of Lipid Vesicles by Cholesterol- and pH-Dependent Assembly of Oligomeric Channels. *Eur. J. Biochem.* **1989**, *181*, 773–773.
23. Floyd, D. L.; Ragains, J. R.; Skehel, J. J.; Harrison, S. C.; van Oijen, A. M. Single-Particle Kinetics of Influenza Virus Membrane Fusion. *Proc. Natl. Acad. Sci. U.S.A.* **2008**, *105*, 15382–15387.
24. Floyd, D. L.; Harrison, S. C.; van Oijen, A. M. Method for Measurement of Viral Fusion Kinetics at the Single Particle Level. *J. Vis. Exp.* **2009**, 48–51.
25. Zaitseva, E.; Yang, S.-T.; Melikov, K.; Pourmal, S.; Chernomordik, L. V. Dengue Virus Ensures Its Fusion in Late Endosomes Using Compartment-Specific Lipids. *PLoS Pathog.* **2010**, *6*, e1001131.
26. Kobayashi, T.; Beuchat, M.-H.; Chevallier, J.; Makino, A.; Mayran, N.; Escola, J.-M.; Lebrand, C.; Cosson, P.; Kobayashi, T.; Gruenberg, J. Separation and Characterization of Late Endosomal Membrane Domains. *J. Biol. Chem.* **2002**, *277*, 32157–32164.
27. Dezi, M.; Di Cicco, A.; Bassereau, P.; Lévy, D. Detergent-Mediated Incorporation of Transmembrane Proteins in Giant Unilamellar Vesicles with Controlled Physiological Contents. *Proc. Natl. Acad. Sci. U.S.A.* **2013**, *110*, 7276–7281.
28. Kahya, N.; Pécheur, E. I.; de Boeij, W. P.; Wiersma, D. a; Hoekstra, D. Reconstitution of Membrane Proteins into Giant Unilamellar Vesicles *via* Peptide-Induced Fusion. *Biophys. J.* **2001**, *81*, 1464–1474.
29. Varnier, A.; Kermarrec, F.; Blesneac, I.; Moreau, C.; Liguori, L.; Lenormand, J. L.; Picollet-D'hahan, N. A Simple Method for the Reconstitution of Membrane Proteins into Giant Unilamellar Vesicles. *J. Membr. Biol.* **2010**, *233*, 85–92.
30. Girard, P.; Pécréaux, J.; Lenoir, G.; Falson, P.; Rigaud, J.-L.; Bassereau, P. A New Method for the Reconstitution of Membrane Proteins into Giant Unilamellar Vesicles. *Biophys. J.* **2004**, *87*, 419–429.
31. Doeven, M. K.; Folgering, J. H. A.; Krasnikov, V.; Geertsma, E. R.; van den Bogaart, G.; Poolman, B. Distribution, Lateral Mobility and Function of Membrane Proteins Incorporated into Giant Unilamellar Vesicles. *Biophys. J.* **2005**, *88*, 1134–1142.
32. Méléard, P.; Bagatolli, L. a; Pott, T. Giant Unilamellar Vesicle Electroformation from Lipid Mixtures to Native Membranes under Physiological Conditions. *Methods Enzymol.* **2009**, *465*, 161–176.
33. Mikelj, M.; Praper, T.; Demič, R.; Hodnik, V.; Turk, T.; Anderluh, G. Electroformation of Giant Unilamellar Vesicles from Erythrocyte Membranes under Low-Salt Conditions. *Anal. Biochem.* **2013**, *435*, 174–180.
34. Chung, M.; Lowe, R. D.; Chan, Y.-H. M.; Ganesan, P. V; Boxer, S. G. DNA-Tethered Membranes Formed by Giant Vesicle Rupture. *J. Struct. Biol.* **2009**, *168*, 190–199.
35. Wang, T.; Ingram, C.; Weisshaar, J. C. Model Lipid Bilayer with Facile Diffusion of Lipids and Integral Membrane Proteins. *Langmuir* **2010**, *26*, 11157–11164.
36. Hamai, C.; Cremer, P. S.; Musser, S. M. Single Giant Vesicle Rupture Events Reveal Multiple Mechanisms of Glass-Supported Bilayer Formation. *Biophys. J.* **2007**, *92*, 1988–1999.
37. Bayley, H. Membrane-Protein Structure: Piercing Insights. *Nature* **2009**, *459*, 651–652.
38. Walker, B.; Krishnasastry, M.; Zorn, L.; Bayley, H. Assembly of the Oligomeric Membrane Pore Formed by Staphylococcal Alpha-Hemolysin Examined by Truncation Mutagenesis. *J. Biol. Chem.* **1992**, *267*, 21782–21786.
39. Walker, B.; Braha, O.; Cheley, S.; Bayley, H. An Intermediate in the Assembly of a Pore-Forming Protein Trapped with a Genetically-Engineered Switch. *Chem. Biol.* **1995**, *2*, 99–105.
40. Kawate, T. Arresting and Releasing Staphylococcal α-Hemolysin at Intermediate Stages of Pore Formation by Engineered Disulfide Bonds. **2003**, 997−1006.
41. Forti, S.; Menestrina, G. Staphylococcal Alpha-Toxin Increases the Permeability of Lipid Vesicles by Cholesterol- and pH-Dependent Assembly of Oligomeric Channels. *Eur. J. Biochem.* **1989**, *181*, 767–773.
42. Geny, B.; Popoff, M. R. Bacterial Protein Toxins and Lipids: Pore Formation or Toxin Entry into Cells. *Biol. Cell* **2006**, *98*, 667–678.
43. Ostolaza, H.; Bartolomé, B.; Ortiz de Zárate, I.; de la Cruz, F.; Goñi, F. M. Release of Lipid Vesicle Contents by the Bacterial Protein Toxin Alpha-Haemolysin. *Biochim. Biophys. Acta* **1993**, *1147*, 81–88.
44. Thompson, J. R.; Cronin, B.; Bayley, H.; Wallace, M. I. Rapid Assembly of a Multimeric Membrane Protein Pore. *Biophys. J.* **2011**, *101*, 2679–2683.
45. Baaken, G.; Sondermann, M.; Schlemmer, C.; Rühe, J.; Behrends, J. C. Planar Microelectrode-Cavity Array for High-Resolution and Parallel Electrical Recording of Membrane Ionic Currents. *Lab Chip* **2008**, *8*, 938–944.
46. Brüggemann, A.; Stoelzle, S.; George, M.; Behrends, J. C.; Fertig, N. Microchip Technology for Automated and Parallel Patch-Clamp Recording. *Small* **2006**, *2*, 840–846.
47. Das, S. K.; Darshi, M.; Cheley, S.; Wallace, M. I.; Bayley, H. Membrane Protein Stoichiometry Determined from the Step-Wise Photobleaching of Dye-Labelled Subunits. *ChemBioChem* **2007**, *8*, 994–999.
48. Kolesinska, B.; Podwysocka, D. J.; Rueping, M. A.; Seebach, D.; Kamena, F.; Walde, P.; Sauer, M.; Windschiegl, B.; Meyer-Ács, M.; Vor der Brüggen, M.; *et al.* Permeation through Phospholipid Bilayers, Skin-Cell Penetration, Plasma Stability, and CD Spectra of A- and B-Oligoproline Derivatives. *Chem. Biodiversity* **2013**, *10*, 1–38.